Green's functions, source signatures, and the normalization of teleseismic wave fields

M. G. Bostock

Department of Earth and Ocean Sciences, University of British Columbia, Vancouver, British Columbia, Canada

Received 3 September 2003; revised 13 December 2003; accepted 24 December 2003; published 10 March 2004.

[1] We examine the canonical source/Green's function separation problem in the context of teleseismic *P* wave scattering from receiver-side crust and upper mantle structure. Conventional "receiver function" analysis affords a leading order approximation to the *S* component of the Green's function but provides no information on *P*-to-*P* scattering. We demonstrate that an improved estimate of the three-dimensional Earth's Green's function, including scattered *P* contributions, can be achieved through consideration of its theoretical spectral properties. Under conditions typical of the real Earth the *P* component of the Green's function is shown to be minimum phase. This behavior is responsible for the success of receiver functions in mantle studies. The minimum-phase property is used here to normalize the source signature on *P* wave seismograms, thereby facilitating implementation of multichannel, multicomponent deconvolution of both Green's function and source signature within the log spectral domain. Examples using both synthetic simulations and seismograms recorded on the Canadian National Seismograph Network illustrate the recovery of accurate and reproducible estimates of the *P* wave Green's function. Our approach can be adapted to a range of source-receiver configurations. In particular, it may prove useful in the recovery of compressional properties beneath portable, field arrays where calibration is provided by nearby, permanent installations. *INDEX TERMS:* 7203 Seismology: Body wave propagation; 7215 Seismology: Earthquake parameters; 7218 Seismology: Lithosphere and upper mantle; 7260 Seismology: Theory and modeling; 7294 Seismology: Instruments and techniques; *KEYWORDS:* Green's functions, deconvolution, teleseismic body waves

Citation: Bostock, M. G. (2004), Green's functions, source signatures, and the normalization of teleseismic wave fields, *J. Geophys. Res.*, *109*, B03303, doi:10.1029/2003JB002783.

1. Introduction

[2] The separation of Earth's impulse response or "Green's function" from source signature is a canonical problem in seismology. In recent years, accurate extraction of the Green's function has become increasingly important in global seismology as researchers rely upon the subtle expression of secondary scattered phases (versus, e.g., travel times of direct waves) to unveil fine-scale structure of the Earth's interior. *P*-to-*S* conversions following in the coda of teleseismic *P* have played a central role in this quest and form the basis of the so-called "receiver-function" approach as pioneered by *Langston* [1979] and *Vinnik* [1977]. In contrast, the use of scattered waves in exploration (or, more generally, active source) seismology has depended in major part on what will be referred to hereafter as "intramodal" scattering wherein incident and scattered waves represent the same mode, that is, predominantly *P*-to-*P* reflection. The basis for this difference in approach arises in the nature of the source. In active-source seismology, the source signature is either known to good approximation (e.g., Vibroseis) or highly localized in time (e.g., dynamite explosive) such that, through processing or by default, the scattered wave field closely resembles the desired Earth's Green's function. As a consequence, the incident *P* wave field in active-source studies can be temporally isolated with relative ease from reflections originating at depth, and deconvolution, although important for target characterization, is directed toward relatively minor modification of wavelet phase.

[3] In contrast, structural studies in global (or passive-source) seismology generally involve the analysis of large earthquakes (magnitudes $\geq$5.6) so as to achieve the signal-to-noise ratios required for characterization of weak contrast lithospheric and mantle discontinuities. Large earthquakes typically exhibit greater rupture areas and evolved time histories over a given frequency band than smaller earthquakes. The length of the source time function for large, shallow events, in particular, may fully overlap with or exceed the time interval over which the Green's function is desired (e.g., first 80 s after direct arrival for most lithospheric/upper mantle studies). For intramodal scattering interactions where both scattered and incident wave types are the same, this temporal overlap exacerbates their separation, especially since the incident wave field generally dominates the scattered waves in amplitude by an order of magnitude or more. Conversions are more easily separated

0148-0227/04/2003JB002783$09.00

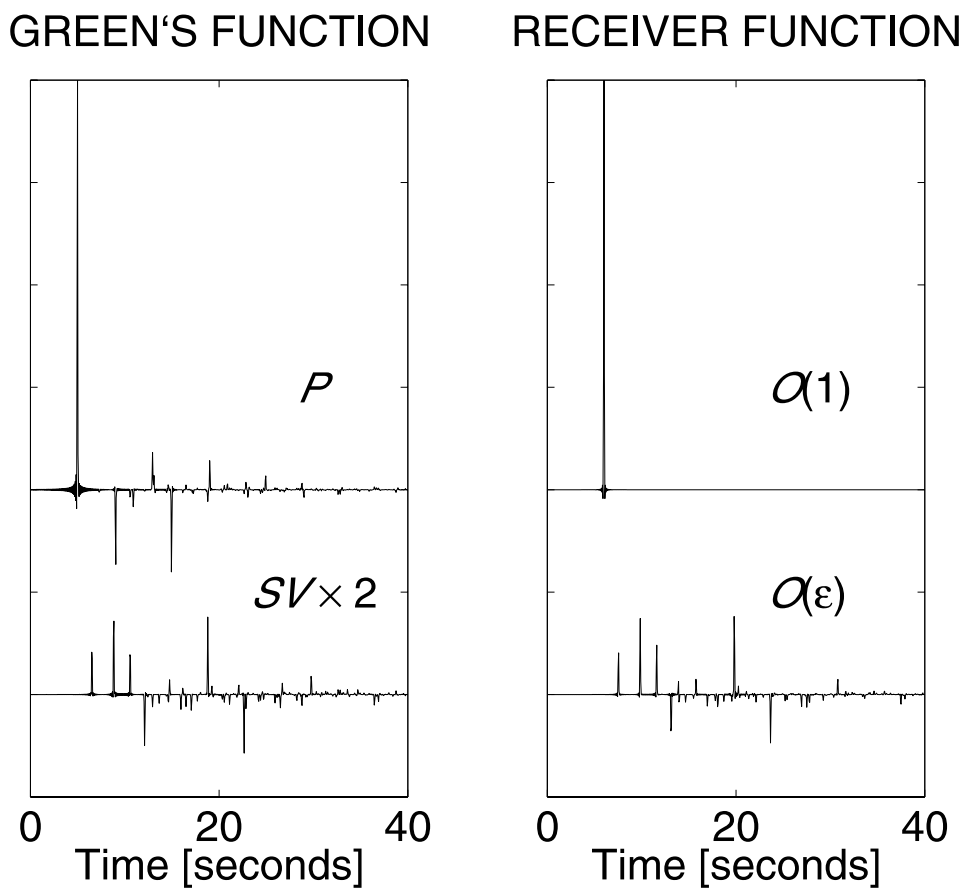

Figure 1. Green's function versus receiver function. (left) P and SV ($\times 2$) response ("Green's function") of an isotropic, two-layer Earth model to an impulsive P wave at precritical slowness. (right) "Receiver function" recovered by deconvolving P and SV components by P component. The receiver function is a leading order approximation to the Green's function correct to zeroth order ($O(1)$) for P and first-order ($O(\epsilon)$) for SV, where ϵ denotes the amplitude of first-order scattering relative to that of the direct wave. Note that $O(\epsilon)$ contributions to the S receiver function are very similar to those of the Green's function, whereas $O(\epsilon^2)$ terms are not.

because the two wave types are orthogonal; that is, P and S waves are curl- and divergence-free, respectively. Stated more simply, any S wave energy observed at the surface due to an incident teleseismic P wave field is by definition scattered, since the arrival of incident S virtually always lies outside of the time interval of interest. Upon isolation of the P and S wave components (and provided that the scattering is weak), a leading order estimate of the Green's function (see Figure 1) can be derived through deconvolution with the P wave signal which comprises dominantly incident wave energy [*Vinnik*, 1977]. The conventional "receiver function" thus represents a crude approximation to this quantity where the P and S wave components are only partly isolated through their approximate association with the vertical and horizontal components of motion, respectively [*Langston*, 1979]. In either case, information on intramodal P scattering is irretrievably lost [see also *Pavlis*, 2003].

[4] Although, mode conversions have served the interests of the research community well as a means for characterizing lithospheric and mantle stratigraphy, there are reasons to consider the use of intramodal P scattering in a global seismological context. Foremost among these is the complementary sensitivity of different scattering interactions to material property contrasts. Whereas conversions (and intramodal S wave interactions) are sensitive primarily to shear-related quantities (e.g., shear velocity, shear impedance), intramodal P wave scattering is controlled by the corresponding compressional properties. Thus characterization of scattered P waves should enable tighter constraints to be placed upon lithological interpretations in global studies. It is also interesting to note that the intramodal P impulse response should be more easily interpretable due to the presence of a single, dominant scattering (free-surface backscattered) mode versus three (one forward scattered, two free-surface backscattered) for the corresponding P-to-S conversion. Ultimately, all scattering interactions (intramode P, S interactions and conversions) are of use in solution of the formal inverse scattering problem wherein (vector) elastic wave data are to be transformed into models of subsurface elastic parameters [*Weglein et al.*, 2003].

[5] In this paper, we will examine the problem of estimating the intramodal scattering signal resulting from interaction of teleseismic P wave fields with near-receiver

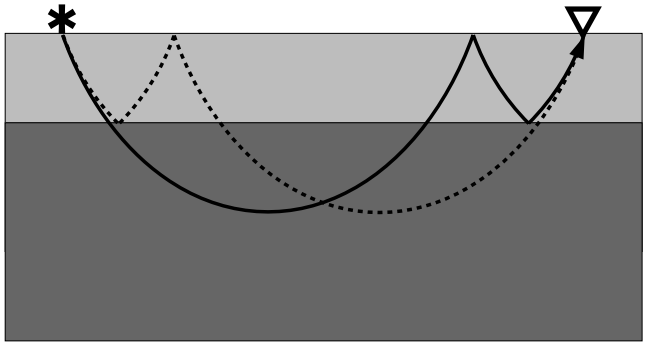

Figure 2. Analogue ray paths. Schematic diagram shows two ray paths that scatter off different structures yet make similar intramodal *P* contributions to the scattered wave field recorded at the receiver.

structure. We are specifically interested in isolating energy reflected from the Earth's free surface and subsequently back scattered from subsurface structure as this is likely to be most useful for imaging purposes. The challenge faced in this task is illustrated in Figure 2, where two schematic ray paths are shown that involve intramodal scattering contributions to a *P* wave seismogram recorded at a surface receiver because of a surface source. The ray path of interest (solid line) scatters *P*-to-*P* from structure on the receiver side, whereas the second path (dashed line) represents near-source *P*-to-*P* scattering. Both scattered waves will arrive within the same time interval at the receiver, and origins of signals on seismogram will be ambiguous, even in the case of an impulsive source signature. Additional information is clearly required if we are to isolate receiver-side scattering from the source-side imprint. This information may be supplied by multichannel measurements. If the scattering structure is localized to the vicinity of an array of receivers and exhibits pronounced lateral variation over the extent of a surface receiver array, then the recorded scattered wave field will exhibit temporal moveout relative to the incident wave field. The wave field scattered from similar structure at the source side displays little moveout relative to the incident wave field and will be considered as part of the source signature. Various forms of time domain stacking [e.g., *Shearer*, 1991; *Revenaugh*, 1995; *Bostock and Rondenay*, 1999a, 1999b] can be used to approximately separate incident and scattered signals when receiver-array measurements are available. If, however, the near-receiver structure presents a dominantly vertical variation in material properties (as is frequently the case) such that scattered waves exhibit little moveout, then array stacking is of little use. Moreover, we note that source estimation via conventional stacking approaches does not honor the convolutional model and will generally result in a loss of higher frequency information.

[6] We shall exploit additional constraints afforded by causality, energy conservation and the convolutional model to improve on these previous efforts to isolate intramodal scattering waves from source signature. The following sections are motivated by the work of *Sherwood and Trorey* [1965], *Claerbout* [1968], and *Ulrych* [1971]. In particular, we demonstrate that, under conditions typical of teleseismic wave propagation in the real Earth, the *P* wave impulse response of receiver-side stratification to an incident *P* wave will be minimum phase. This property is important as it provides a means of normalizing teleseismic recordings that is amenable to multichannel deconvolution of the Green's function and source signatures within the log spectral domain. These concepts are illustrated through applications to both synthetic simulations and data recorded from the Canadian National Seismograph Network (CNSN).

2. Minimum Phase and Teleseismic Wave Fields

[7] Our focus in this section is to examine the spectral properties of the transfer operator that describes the response of a one-dimensional (1-D) stratified, isotropic, elastic half-space to an incident plane *P* wave. In particular we wish to assess to what degree the operator can be characterized as minimum phase. As depicted in Figure 3, the stratification comprises k layers overlying a homogeneous half-space at z_k and bounded above by the free surface at $z = 0$. An impulsive plane *P* wave, incident from below, is characterized by horizontal slowness p and radial frequency ω. Since the stratification is laterally homogeneous, p and ω are the same for all scattering interactions within the stratification. We will further assume that all wave fields are propagating; that is, there are no evanescent waves. Following a notation convention adapted from that of *Kennett* [1983], the time- and amplitude-normalized upgoing wave vector $\hat{\mathbf{w}}_U$ recorded at the free surface is related to the incident wave field below the stratification through a transfer matrix $\hat{\tilde{\mathbf{T}}}_U = \hat{\tilde{\mathbf{T}}}_U(p,\omega)$ as

$$\hat{\mathbf{w}}_U = \begin{bmatrix} \hat{w}_U^P \\ \hat{w}_U^V \end{bmatrix} = \hat{\tilde{\mathbf{T}}}_U \begin{bmatrix} 1 \\ 0 \end{bmatrix}, \tag{1}$$

where the two elements of the wave vectors are ordered as *P* and *SV* waves. An analogous scalar relation could be written for *SH* waves, and a third dimension would be required for media exhibiting elastic anisotropy. The transfer operator can be written as

$$\hat{\tilde{\mathbf{T}}}_U = \left[\mathbf{I} - \mathbf{R}_D\tilde{\mathbf{R}}\right]^{-1}\mathbf{N}_U\mathbf{T}_U, \tag{2}$$

where $\mathbf{I}$ is the identity matrix, $\mathbf{R}_D$ is the reflection matrix for downward incidence upon the stratification (without the free

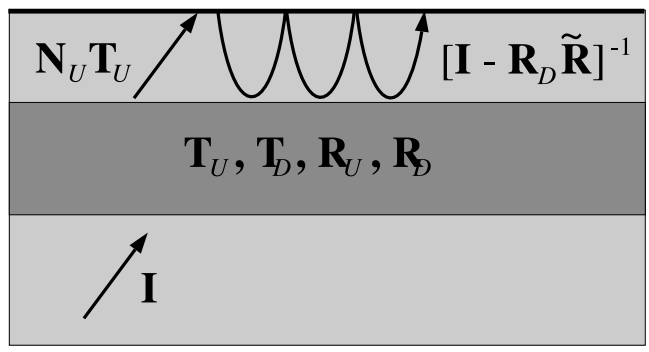

Figure 3. Stratified half-space. One-dimensional Earth model and quantities used to characterize spectral properties of transfer operator $\hat{\tilde{\mathbf{T}}}_U(p,\omega)$ that describes impulse response for incident plane *P* wave.

surface), $\mathbf{T}_U$ is the transmission matrix for the stratification (without the free surface), $\tilde{\mathbf{R}}$ is the free surface reflection matrix and $\mathbf{N}_U$ is a matrix defined as

$$\mathbf{N}_U = \mathbf{N}_U(0, z_k) = \frac{e^{i\omega\left(\sum_{i=1}^{k} \Delta z_i \sqrt{\alpha_i^{-2} - p^2}\right)}}{\prod_{i=1}^{k} \bar{T}_{U_i}^{PP}} \mathbf{I}. \tag{3}$$

In equation (3), α_i is the P velocity within the ith layer, $\bar{T}_{U_i}^{PP}$ is the upward P wave transmission coefficient across the base of the ith layer, and Δz_i is the thickness of the ith layer. Thus $\mathbf{N}_U$ reduces the first (P) arrival to unit amplitude and repositions it to zero time. The quantity $[\mathbf{I} - \mathbf{R}_D\tilde{\mathbf{R}}]^{-1}$ is the reverberation operator that accounts for the infinite sequence of multiple reflections set up between the free surface and underlying structure. At this point we note that the wave vector $\hat{\mathbf{w}}_U$ can be readily computed from surface observations of particle displacement or velocity assuming knowledge of slowness and wave velocities at the surface, for both the impulsive source implied in (1) and more general source signatures [*Kennett*, 1991].

[8] In this and the following sections, we shall exploit the constraints that reciprocity and energy conservation place upon the nature of the upgoing P wave field recorded at the surface. Without loss of generality, it will be convenient to normalize the reflection/transmission matrices by vertical energy flux [*Kennett*, 1983] and note, then, that

$$\mathbf{R}_D = \mathbf{R}_D^{\mathrm{T}}, \quad \mathbf{R}_U = \mathbf{R}_U^{\mathrm{T}}, \quad \mathbf{T}_U = \mathbf{T}_D^{\mathrm{T}} \tag{4}$$

by reciprocity and, recalling our stipulation that all wave fields are propagating,

$$\mathbf{I} = \mathbf{R}_D^{\dagger}\mathbf{R}_D + \mathbf{T}_D^{\dagger}\mathbf{T}_D = \mathbf{R}_U^{\dagger}\mathbf{R}_U + \mathbf{T}_U^{\dagger}\mathbf{T}_U, \tag{5}$$

by energy conservation, where superscript T and superscript dagger denote transpose and complex-conjugate transpose, respectively.

[9] We turn our attention now to the spectral characteristics of $\hat{\tilde{\mathbf{T}}}_U$ and, specifically, the first element on the diagonal, $\hat{\tilde{T}}_U^{PP}$, that describes intramodal P-P scattering. In recognition that the wave field $\hat{\mathbf{w}}_U$ will be discretely sampled at time intervals Δt and without loss of generality, we shall elect to consider all quantities in (2) in the Z transform domain. The individual elements in each matrix thus become polynomials in Z and we are able to simultaneously examine their properties in the time and frequency domains. The time series is identified in the coefficients of powers of Z, whereas summation of the polynomial with $Z = e^{i\omega\Delta t}$ yields the frequency domain form. To proceed, we write the reverberation operator as a product of the adjoint and determinant of its inverse:

$$\left[\mathbf{I} - \mathbf{R}_D\tilde{\mathbf{R}}\right]^{-1} = \mathbf{X}^{-1} = \frac{\mathrm{adj}(\mathbf{X})}{\det|\mathbf{X}|}. \tag{6}$$

For P-SV propagation in isotropic media the quotient can be written explicitly as

$$\frac{\mathrm{adj}(\mathbf{X})}{\det|\mathbf{X}|} = \frac{1}{X^{PP}X^{VV} - X^{PV}X^{VP}} \begin{bmatrix} X^{VV} & -X^{VP} \\ -X^{PV} & X^{PP} \end{bmatrix}, \tag{7}$$

where the individual elements of $\mathbf{X}$ are defined as

$$X^{PP} = 1 - R_D^{PP}\tilde{R}^{PP} - R_D^{PV}\tilde{R}^{VP}$$

$$X^{PV} = -R_D^{PP}\tilde{R}^{PV} - R_D^{PV}\tilde{R}^{VV}$$

$$X^{VP} = -R_D^{VP}\tilde{R}^{PP} - R_D^{VV}\tilde{R}^{VP}$$

$$X^{VV} = 1 - R_D^{VP}\tilde{R}^{PV} - R_D^{VV}\tilde{R}^{VV}.$$

All elements of $\mathbf{X}$, $\mathbf{R}_D$, and $\tilde{\mathbf{R}}$ are causal, that is, they represent polynomials with powers of Z greater than or equal to zero. In particular, the elements of $\mathbf{R}_D$ comprise powers of Z greater than or equal to 2 assuming that the P transit time through the shallowest layer in the stratification is equal to or greater than the sample interval. From equation (5), the magnitudes of elements of $\mathbf{R}_D$ are less than unity at all frequencies. Moreover, the free-surface reflection matrix $\tilde{\mathbf{R}}$ is unitary, i.e., $\tilde{\mathbf{R}}^{\dagger}\tilde{\mathbf{R}} = \mathbf{I}$, and its elements involve only coefficients of $Z^0 = 1$ since there is no time delay involved in its action. To proceed, we recall the following properties of Z-transformed time series [*Claerbout*, 1976]: (1) a unit impulse at zero delay (i.e., unit coefficient of Z^0) is minimum phase; (2) the convolution of two minimum-phase time series is a minimum-phase time series; (3) the inverse of a minimum-phase time series is minimum phase; and (4) the sum of a minimum-phase time series with a second time series that is nonminimum phase is itself minimum phase if the power spectrum of the second series is less than that of the first at all frequencies. Upon consideration of properties 1-4 and the aforementioned properties of the reflection matrices $\mathbf{R}_D$, $\tilde{\mathbf{R}}$, we see that all of X^{PP}, X^{VV}, det $|\mathbf{X}|$, and the diagonal elements of $[\mathbf{I} - \mathbf{R}_D\tilde{\mathbf{R}}]^{-1}$ must represent minimum-phase time series. Moreover, we recall that the diagonal elements of the free-surface reverberation operator are those that contribute to intramodal (both P-to-P and SV-to-SV) scattering interactions.

[10] Having established the minimum-phase characteristics of the free-surface reverberation operator, it remains to analyze the properties of the second factor on the right-hand side of equation (2) $\mathbf{N}_U\mathbf{T}_U$. This quantity represents the normalized transmission matrix for upward incidence upon the stratification in the absence of a free surface. It has long been known [*Sherwood and Trorey*, 1965] that $\mathbf{N}_U\mathbf{T}_U$ is minimum phase for scalar acoustic waves at vertical incidence. Let us demonstrate this property by considering the form that $\mathbf{N}_U\mathbf{T}_U$ takes in 1-D isotropic media for $p = 0$. In this case P and SV waves are decoupled and all necessary quantities can be represented by scalars (identified here by italic font). We begin by considering the transmission response for a single layer embedded within a whole-space between depths z_1 and z_2,

$$T_U^{PP} = \bar{T}_{U_1}^{PP}\left[1 - E^{PP}\bar{R}_{D_2}^{PP}E^{PP}\bar{R}_{U_1}^{PP}\right]^{-1}E^{PP}\bar{T}_{U_2}^{PP}, \tag{8}$$

where $E^{PP} = e^{-i\omega\Delta z_2/\alpha_2}$ represents the phase income for a single transit through the layer, and, for example, the quantity $\bar{R}_{U_1}^{PP}$ represents the upward P-to-P reflection coefficient for the interface at z_1 (evaluated at vertical incidence in this instance). Multiplying by the scalar

normalization factor $N_U(z_1, z_2) = e^{-i\omega\Delta z_2/\alpha_2}/\bar{T}_{U_1}^{PP}\bar{T}_{U_2}^{PP}$ (see equation (3)) for the layer yields

$$N_U T_U^{PP} = \left[1 - E^{PP}\bar{R}_{D_2}^{PP}E^{PP}\bar{R}_{U_1}^{PP}\right]^{-1}, \tag{9}$$

and using arguments analogous to those employed above for the free-surface reverberation operater, we see that the quantity $N_U T_U^{PP}$ must be minimum-phase. By invoking the addition rule for transmission matrices [*Kennett*, 1983], generally stated as

$$\mathbf{T}_U(z_1, z_k) = \mathbf{T}_U(z_1, z_j)\left[\mathbf{I} - \mathbf{R}_D(z_j, z_k)\mathbf{R}_U(z_1, z_j)\right]^{-1}\mathbf{T}_U(z_j, z_k) \tag{10}$$

where $z_1 < z_j < z_k$, we may then extend this argument by recursion to show that the impulse response $N_U T_U^{PP}$ is minimum phase for P waves at normal incidence in arbitrary 1-D isotropic stratification. Since the convolution of two minimum-phase time series is minimum phase (property 2), the total transfer operator $\hat{\bar{T}}_U^{PP} = [I + R_D^{PP}]^{-1}N_U T_U^{PP}$ (where we have used the fact that the free-surface reflection coefficient is -1 for P waves at normal incidence) is also minimum phase. This result carries over to *SV* waves at vertical incidence and *SH* waves at precritical values of slowness p.

[11] The argument presented above for vertical incidence will not, however, hold generally at nonzero horizontal slowness in 1-D media. This is most readily evident in the case of a single layer for which equation (8) generalizes to

$$\mathbf{T}_U = \bar{\mathbf{T}}_{U_1}[\mathbf{I} - \mathbf{E}\bar{\mathbf{R}}_{D_2}\mathbf{E}\bar{\mathbf{R}}_{U_1}]^{-1}\mathbf{E}\bar{\mathbf{T}}_{U_2}, \tag{11}$$

where $\bar{\mathbf{R}}_{D_i}$, $\bar{\mathbf{R}}_{U_i}$, $\bar{\mathbf{T}}_{U_i}$ are interfacial reflection and transmission matrices for boundary at depth z_i, and the elements of the diagonal matrix $\mathbf{E}$ are the phase incomes of P and *SV* waves through the layer. Noting that the reverberation term can be expanded as an infinite series, we find that the complication arises as a result of contributions to the *PP* element of $\mathbf{T}_U$ from the lowest-order term $\bar{T}_{U_1}^{PV}E^{VV}\bar{T}_{U_2}^{VP}$ which represents entirely forward propagating energy that has converted from P to *SV* at the lower interface and back to P across the upper interface. In 1-D media exhibiting extreme material property contrasts and at larger (but nonetheless precritical) slownesses, the conversion coefficients $\bar{T}_U^{PV}$, $\bar{T}_U^{VP}$ can exceed the intramodal transmission coefficients $\bar{T}_U^{PP}$ resulting in delayed, doubly converted arrivals that are greater than the direct wave in amplitude and, more specifically, violate the condition of minimum phase expressed in property 4 above. Consequently, the P impulse response $\hat{w}_U^P$ at nonzero slowness is no longer guaranteed to be minimum phase.

[12] A development analogous to that just presented for P waves can also be made for *SV* waves. We have already shown that the diagonal element of the free-surface reverberation operator corresponding to intramodal *SV* interaction is minimum phase. To address the transmission operator $\mathbf{N}_U\mathbf{T}_U$, the normalization matrix $\mathbf{N}_U$ in equation (3) must be redefined in terms of the corresponding shear velocity and *SV* transmission coefficients. For $p \neq 0$, this operator is never minimum phase in any vertically heterogeneous model due to the acausal (relative to the arrival of the direct wave) contributions to the *SV* component waveform arising through *SV*-to- *P*-to-*SV* scattering interactions. For realistic Earth models these second-order scattering interactions will, however, be small and, in the context of linearized inverse scattering, negligible. The situation deteriorates for shear waves in anisotropic media where strong qS coupling [*Coates and Chapman*, 1990] represented by large off-diagonal elements in $\mathbf{T}_U$ will result in surface recordings with a decidedly mixed-phase character.

3. Generalization and Normalization

[13] Despite the fact the P impulse response $\hat{w}_U^P$ for precritical incidence in arbitrary 1-D stratification is not guaranteed to be minimum phase, numerical experiments confirm that it is so for an overwhelming majority of plausible 1-D lithospheric and upper mantle Earth models at slownesses corresponding to teleseismic distances ($p \leq 0.08$ s k m^{-1}). Physically, this property is due to the fact that the direct arrival at zero time is significantly more energetic than the reverberations that follow in its wake (see property 4) of the previous section). Accordingly, we expect the same behavior to persist for teleseismic P wave propagation in most realistic, laterally heterogeneous Earth models. In substantive support of this latter contention, we note that traditional "receiver function analysis" would produce uninterpretable results were it not for the minimum-phase character typical of real Earth transmission responses because a nonminimum phase P component would no longer afford a useful approximation to the source signature $S(\omega)$. The success of receiver functions in studies of deep Earth structure is therefore testament to the minimum-phase character of teleseismic P wave fields. Stated in a more quantitative fashion, the P contribution to the 3-D Earth's Green's function at teleseismic distances is generally minimum phase because the energy in the incident wave (i.e., the impulsive first arrival) is generally greater than that of the scattered wave field that follows, at all frequencies.

[14] Violations to the minimum-phase assumption may occur in certain circumstances. For example the generation of multiply scattered *P*-to- *S*-to-*P* forward conversions at near critical slownesses, as described in the previous section, might occur in areas where stations are located over thick sedimentary sequences. The development of caustics, such as those that occur at greater regional distances (and $p >$ 0.08 s k m^{-1}) due to the transition zone (410 and 660 km) discontinuities may also produce nonminimum phase responses. Provided that all scattering interactions are precritical, a plane-wave decomposition can, in principle, be used to separate the interfering components which should individually possess the minimum-phase property. Caustics generated by complex laterally heterogeneous structures will be more difficult to address but should occur infrequently and, again, only at higher frequencies (>1 Hz) and larger slownesses.

[15] The minimum-phase character of the teleseismic response is important for the purpose of analyzing intramodal scattering. If the transmission impulse response is assumed to be minimum-phase, then, from property 2 of the previous section, the nonminimum phase component of an observed P component seismogram must originate exclu-

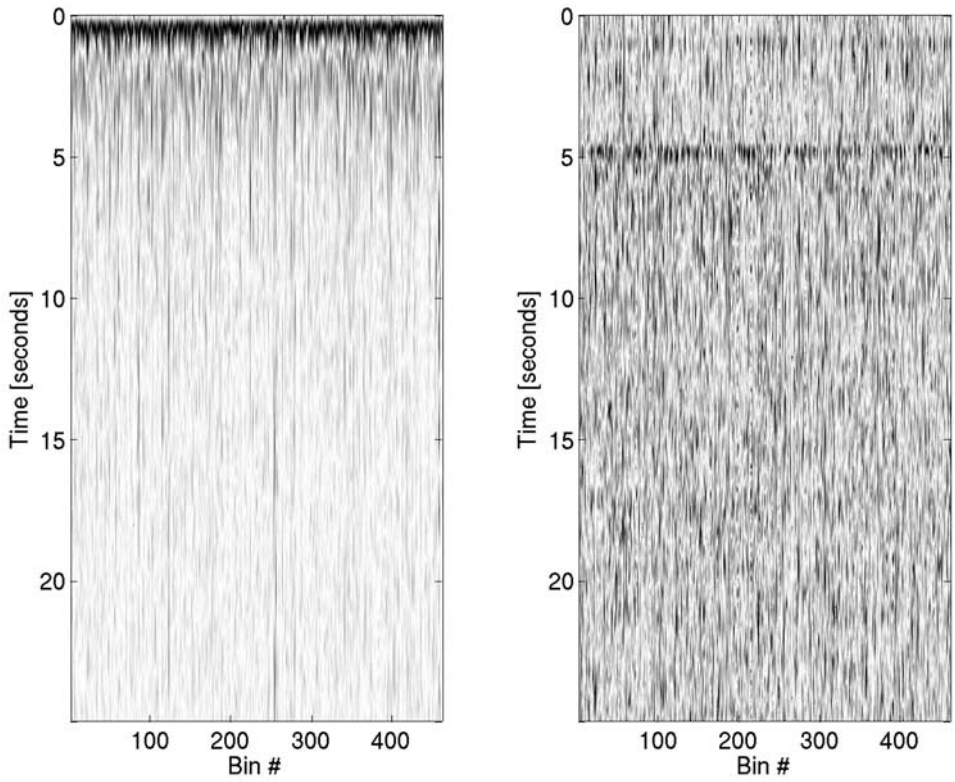

Figure 4. Normalization by minimum phase. (a) *P* and (b) *S* wave sections for 461 seismograms recorded at station YKW3 normalized to minimum phase. Note the definition of Moho converted phase in Figure 4b at 5 s. *P* section is dominated by incident wave at zero time.

sively within the source signature $S(\omega)$. We recognize then that by transforming an observed seismogram to minimum phase, we construct, in effect, the seismogram that would have been recorded for a minimum-phase source with the same power spectrum as the original source. Since a minimum-phase waveform has more energy concentrated at early times than any other waveform sharing its spectrum [*Robinson and Treitel*, 1980], transformation of a *P* component seismogram to minimum phase can be viewed as the application of an all-pass "shaping filter" that "normalizes" the seismogram (or, more precisely the source signature) and thus serves to emphasize discrete arrivals.

[16] The shaping filter derived through minimum-phase transformation of a *P* component seismogram may also be applied to nonminimum-phase data sharing the same source spectrum. The most obvious candidates are the *SV* and *SH* components (or *qS*1 and *qS*2) components of the same three-component seismogram. The all-pass shaping filter $A(\omega)$ is simply defined using the observed, frequency-domain *P* component seismogram $S(\omega)w_U^P(\omega)$ (the lack of caret on w_U^P signifies that the data need not be normalized in amplitude nor time) as

$$A(\omega) = \frac{\mathcal{K}\{S(\omega)w_U^P(\omega)\}}{S(\omega)w_U^P(\omega)} = \frac{\mathcal{K}\{S(\omega)\}w_U^P(\omega)}{S(\omega)w_U^P(\omega)} = \frac{\mathcal{K}\{S(\omega)\}}{S(\omega)} \quad (12)$$

where transformation to minimum phase is denoted by $\mathcal{K}\{\}$ and is most efficiently performed using the Kolmogorov algorithm [*Kolmogorov*, 1939; *Claerbout*, 1976]. Frequency-domain multiplication of the remaining (mixed phase) wave vector components by this filter produces waveforms that correspond to the same minimum-phase source. To demonstrate application we plot the minimum-phase normalized *P* and *SV* components for a data set of 461 seismograms recorded at the Yellowknife Seismic Array (YKW3) in Canada's Northwest Territories in Figure 4. Seismograms are plotted in gray scale and ordered in slowness (or decreasing epicentral distance). Coherent energy can be traced across the *SV* plot at times of ~5 s and (to a lesser degree) 15 and 20 s corresponding to direct and free-surface reflected conversions generated at the continental Moho. These features are not as well defined as they would be had a proper (e.g., receiver-function) deconvolution been performed because only the phase spectrum (and not the amplitude spectrum) is affected. As a result, pulse widths of individual arrivals are more variable trace to trace. A second consequence of the variable amplitude spectra is the presence of subsidiary lobes following the main peak of an arrival. Their effect is most obvious on the *P* section due to the dominance of the direct *P* wave at zero time. This arrival is larger by an order of magnitude or more than the scattered signals we wish to isolate (e.g., the topside *P*-to-*P* reflection from the continental Moho) and the secondary lobes obscure energy arriving in at least the following 10-20 s. To achieve better isolation of the scattered signals, we could stack seismograms along expected moveout curves for 1-D velocity models [e.g., *Vinnik*, 1977]. Large numbers of seismograms are, however, required for this purpose, and the stacking

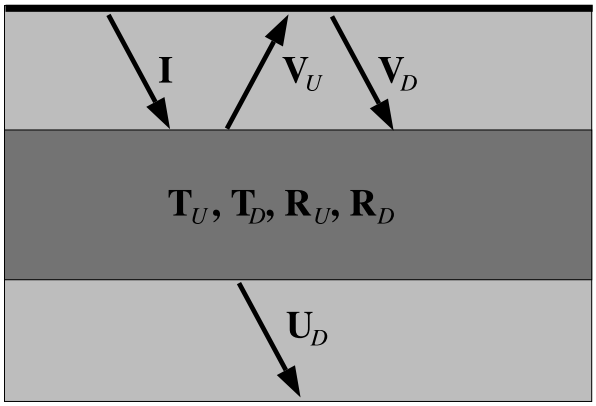

a)

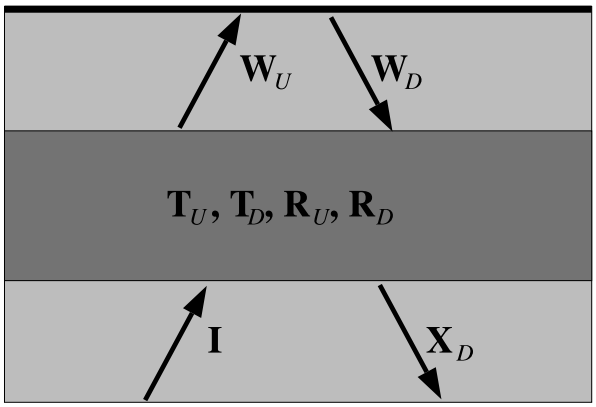

b)

Figure 5. Definition of quantities used to define the transformation of a plane wave reflection experiment to a plane wave transmission experiment.

process invariably distorts the Green's function through attenuation of high frequencies, thereby destroying valuable information concerning 3-D structure. In a later section, we examine a means of more effectively isolating the source and Green's function contributions that exploits both the convolutional model and the transformation of a *P* seismogram to minimum phase. We will use the term minimum-phase "normalization" hereafter to refer to this transformation because it renders the inherent source signature strongly peaked and positive near time $t = 0$.

4. Normalization by Autocorrelation

[17] In this section we examine a correlation-based normalization of the wave field, due to *Claerbout* [1968] [see also *Frasier*, 1970; *Wapenaar et al.*, 2004], that is closely related to the minimum-phase normalization discussed in section 3. In this approach we consider first the response of our stratified half-space to incident impulsive, plane *P* and *S* wave fields (at constant ω, p) excited at the free surface (Figure 5) through the prescription of a source wave vector matrix **I**. This source will give rise to upgoing and downgoing wave fields at the surface represented by wave vector matrices $\mathbf{V}_U$ and $\mathbf{V}_D$ and a downgoing wave field in the homogeneous half-space below the stratification given by another wave vector matrix $\mathbf{U}_D$. These quantities can be written in terms of the reflection/transmission matrices for the stratified region as

$$\mathbf{V}_U = \left[\mathbf{I} - \mathbf{R}_D\tilde{\mathbf{R}}\right]^{-1}\mathbf{R}_D \tag{13}$$

$$\mathbf{V}_D = \mathbf{I} + \tilde{\mathbf{R}}\left[\mathbf{I} - \mathbf{R}_D\tilde{\mathbf{R}}\right]^{-1}\mathbf{R}_D = \mathbf{I} + \tilde{\mathbf{R}}\mathbf{V}_U \tag{14}$$

$$\mathbf{U}_D = \mathbf{T}_D\left[\mathbf{I} + \tilde{\mathbf{R}}\left[\mathbf{I} - \mathbf{R}_D\tilde{\mathbf{R}}\right]^{-1}\mathbf{R}_D\right] = \mathbf{T}_D\mathbf{V}_D. \tag{15}$$

Assuming, as before, precritical slowness and elastic media, vertical energy flux is conserved in depth. Thus we may set the flux at the surface and lower boundary of the stratification to be equal, such that

$$\mathbf{V}_D^\dagger\mathbf{V}_D - \mathbf{V}_U^\dagger\mathbf{V}_U = \mathbf{I} + \tilde{\mathbf{R}}\mathbf{V}_U + \mathbf{V}_U^\dagger\tilde{\mathbf{R}}^\dagger = \mathbf{U}_D^\dagger\mathbf{U}_D. \tag{16}$$

Now consider the reciprocal experiment where the impulsive incident wave field is incident upon the stratification from below and we represent the wave field at the surface by a wave vector matrix $\mathbf{W}_U$ comprising the two upgoing column wave vectors that represent the impulse response to the incident *P* wave and *S* wave sources. By reciprocity and in analogy with the third equation in equation (4), we have $\mathbf{W}_U = \mathbf{U}_D^{\mathrm{T}}$ so that

$$\mathbf{W}_U^*\mathbf{W}_U^{\mathrm{T}} = \mathbf{I} + \tilde{\mathbf{R}}\mathbf{V}_U + \mathbf{V}_U^\dagger\tilde{\mathbf{R}}^\dagger, \tag{17}$$

where the asterisk signifies complex conjugate. The quadratic form comprising complex conjugate waveforms on the left-hand side of equation (17) implies sums of autocorrelations and cross correlations of seismograms in the time domain and, further, indicates that by measuring the appropriate responses (i.e., due to both *P* and *S* sources at constant p) for the earthquake geometry (i.e., plane wave from below), one may recover the result of a reflection experiment, namely, $\mathbf{V}_U$, for which the source wave field is incident from above. For normal incidence in isotropic media *P* and *SV* interactions are decoupled and so only autocorrelations of single component wave fields are required.

[18] The same derivation could have been carried out with a more general source $S(\omega)\mathbf{I}$, in which case both sides of equation (17) would be multiplied by the power spectrum of the source, $S^*(\omega)S(\omega)$ implying convolution with a new source time signature in the time domain. This source time signature is the zero-phase, autocorrelation of the original source and can therefore be viewed as a normalization of the wave field in much the same way as transformation to minimum phase. That is, the autocorrelation of the source will, in general, be more strongly peaked than that of the original source (a property exploited in global seismology by, for example, *Shearer* [1991]), and hence secondary scattered arrivals more easily identified and isolated. The relevant Green's function is no longer that corresponding to a transmission response but rather that for a plane-wave

reflection response. From a practical point of view, normalization by autocorrelation, as presented above, is rather less attractive than transformation to minimum phase for a number of reasons. Strictly speaking, the procedure requires measurements from two separate experiments, involving individual P and S wave sources at the same value of horizontal slowness p with the same source signature. This requirement cannot be easily met in practice, although, for small slownesses corresponding to more distant teleseismic sources the wave-coupling contributions (i.e., cross correlations) in equation (17) are small and may be ignored. More serious perhaps is the extension to multiple dimensions. *Wapenaar et al.* [2004] have demonstrated how *Claerbout*'s [1968] result generalizes to three dimensions. The generalization involves integrals of cross-correlated transmission responses due to point sources distributed below the deepest interface of interest, a scenario that may be difficult to accommodate for teleseismic observations.

[19] Within the context of vertical incidence in 1-D isotropic, elastic media where both normalization by minimum phase and autocorrelation retain full validity, it is interesting to note that autocorrelation of the transmission response due to incidence from below the stratification yields the reflectivity due to incidence from above, yet transformation to minimum phase only alters the effective source signature of the transmission response. Indeed, the two responses are qualitatively very similar (at least for the modest contrasts displayed by normal lithospheric/upper mantle models) as might perhaps have been surmised from a comparison of equation (2) with equations (13)–(17). The primary difference would appear to be the reorganization of reverberations internal to the stratification (i.e., independent of the free surface) induced in transmission to those created by reflection, which, in general, have very different kinematic behaviors. This reorganization is somehow accomplished by the action of correlation.

5. Multichannel Deconvolution

[20] As we have argued in section 3, transformation of teleseismic P seismograms to minimum phase normalizes the source signature such that the intramodal scattering component of an underlying 3-D Green's function is more readily identifiable. The effect of the source (including source-side scattering) is still significant, however, and, as noted in Figure 4, sufficient, in general, to obscure the weaker (receiver-side) intramodal-scattered arrivals that are likely to be of most interest in structural studies. In this section we present a methodology for producing accurate estimates of both source signatures and 3-D Green's functions that exploits multichannel recordings within the convolutional model, and the properties of minimum-phase time series.

[21] We consider a collection of $M \times N$ minimum-phase normalized P component recordings representing M sources measured by N receivers. In constructing the P component from a three-component displacement/velocity seismogram, our main requirement is that it contain as much of the incident P wave field energy as possible. This may be accomplished using the wave field decomposition schemes of *Kennett* [1991], *Vinnik* [1977], or, less desirably, simply through selection of the vertical component seismogram. The $m \times n$th seismogram is then written in the frequency domain as

$$P_{mn}(\omega) = S_m(\omega) G_n(\omega), \tag{18}$$

where $S_m(\omega)$ is mth source signature and $G_n(\omega)$ is the impulse response or Green's function at the nth receiver. By taking logarithms we can turn this multiplicative relation into an additive one,

$$\log\{P_{mn}(\omega)\} = \log\{S_m(\omega)\} + \log\{G_n(\omega)\}, \tag{19}$$

and thereby cast the multichannel convolution as a system of linear equations involving the same matrix relation for each frequency. Consider, for example, $M = 3$, $N = 2$ for which we can write

$$\begin{bmatrix} 1 & 0 & 0 & 1 & 0 \\ 1 & 0 & 0 & 0 & 1 \\ 0 & 1 & 0 & 1 & 0 \\ 0 & 1 & 0 & 0 & 1 \\ 0 & 0 & 1 & 1 & 0 \\ 0 & 0 & 1 & 0 & 1 \end{bmatrix} \begin{bmatrix} \log\{S_1(\omega)\} \\ \log\{S_2(\omega)\} \\ \log\{S_3(\omega)\} \\ \log\{G_1(\omega)\} \\ \log\{G_2(\omega)\} \end{bmatrix} = \begin{bmatrix} \log\{P_{11}(\omega)\} \\ \log\{P_{12}(\omega)\} \\ \log\{P_{21}(\omega)\} \\ \log\{P_{22}(\omega)\} \\ \log\{P_{31}(\omega)\} \\ \log\{P_{32}(\omega)\} \end{bmatrix}. \tag{20}$$

Although we have $M \times N$ equations in $M + N$ unknowns, it is easily verified that the system has rank $M + N - 1$, and thus we require an additional constraint if it is to be solved by standard least squares minimization. This constraint could be supplied in a variety of forms. For example, if an estimate of a single source signature or receiver response is available, its incorporation renders the system full rank; however, the accuracies of all other recovered $S_m(\omega)$, $G_n(\omega)$ then hinge directly on this estimate. We can more conservative by exploiting our normalization of the data $P_{mn}(\omega)$. In the limits of an infinite number of independent sources and of full-band data, one would expect the cumulative product of minimum-phase normalized source spectra to tend toward a real constant in frequency,

$$\lim_{M\to\infty} \left[\prod_m^M S_m(\omega) \right]^{\frac{1}{M}} \equiv \lim_{M\to\infty} \frac{1}{M} \sum_m^M \log\{S_m(\omega)\} = C, \tag{21}$$

that is, a delta function in the time domain. We recall that a delta function is minimum phase as befits the normalization. The burden of fulfilling this last constraint, written for the system in equation (20) as

$$\begin{bmatrix} 1/M & 1/M & 1/M & 0 & 0 \end{bmatrix} \begin{bmatrix} \log\{S_1(\omega)\} \\ \log\{S_2(\omega)\} \\ \log\{S_3(\omega)\} \\ \log\{G_1(\omega)\} \\ \log\{G_2(\omega)\} \end{bmatrix} = [C], \tag{22}$$

is now shared among all source spectra and there is thus greater prospect for recovering a reliable solution. In practice, we will have both finite bandwidth and, as above, a finite number of sources. The qualitative effect of these limitations can be gauged by considering, for example, an experiment with equal numbers of sources and receivers where each receiver records each source, and for which the

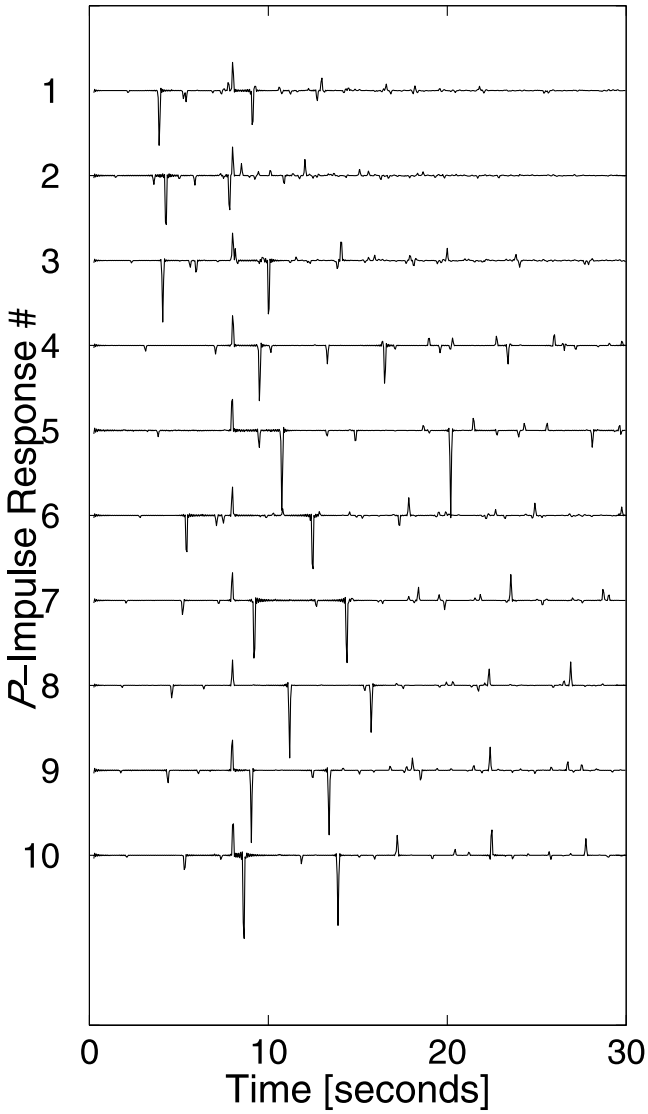

Figure 6. Synthetic P impulse response. The impulse response for 10 crustal models normalized to the arrival time of the direct wave are shown. An unphysical arrival at $t = 8.0$ s relative to the direct wave is added to the response at all stations. See text for details.

constant C in equation (21) is set to 0 (the constant simply trades off the relative magnitude of sources with respect to impulse responses). In this case, we implicitly set the sum of the log spectral impulse responses to equal the sum of the log spectra of the data, that is

$$\sum_{n}^{N} \log\{G_n(\omega)\} = \sum_{m}^{M} \sum_{n}^{N} \log\{P_{mn}(\omega)\}. \tag{23}$$

Thus we expect the recovered impulse responses to possess amplitude spectra similar to those of the data. Moreover, any signal within the source log spectra that is common to all events will be incorrectly assigned to the recovered Green's functions.

[22] A second possible constraint equation involves setting the sum of the Green's function log spectra to a constant, e.g.,

$$\sum_{n}^{N} \log\{G_n(\omega)\} = 0. \tag{24}$$

In this case we force full bandwidth upon the Green's function solution (a reasonable expectation) but also assume that Earth structure at all stations is independent. Thus any signal within the log spectra of $G_n(\omega)$ that is common to all stations will be falsely mapped to the source estimates. The application, that is either source signature estimation or Green's function recovery, will dictate the appropriate choice of constraint. In general, we expect that source signatures will be more independent than receiver impulse responses. That is, although earthquake moment tensors for a given source region will tend to be highly correlated, their associated time functions will depend on the intricate details of the local stress regime and source position relative to major local structures (e.g., free surface), both of which will change from event to event. In contrast, we can expect a common spectral component to exist across many receivers in structural studies. For example, most continental receiver responses will exhibit a crust-mantle boundary between 30 and 40 km depth whose identification and characterization will be important in geologic/geodynamic interpretations. We therefore advocate the use of equation (21) for structural studies, though we must recognize the potential for residual source contamination. For source studies the constraint in equation (24) may be more appropriate. The original source signatures can be retrieved through deconvolution of the normalized forms $S_m(\omega)$ with the shaping filters $A_{mn}(\omega)$ used to transform P_{mn} (see equation (12)) or through some form of multichannel averaging involving deconvolution of the $A_{mn}(\omega)$ from $P_{mn}(\omega)$ with care taken to account for relative time delays among the raw P seismograms.

[23] Before proceeding, it should be emphasized that normalization by minimum phase also obviates a major complication that has plagued earlier attempts to exploit the construction in equation (19) [*Ulrych*, 1971; *Clayton and Wiggins*, 1976; *Crosson and Dewberry*, 1994; *Bostock and Sacchi*, 1997], namely, the unwrapping of phase. The imaginary component of complex quantities in the log spectral domain corresponds to the phase of their frequency spectra. The phase spectrum of an arbitrary signal exhibits a monotonic trend with frequency that must be reconstructed (or "unwrapped") from the phase modulo $2\pi\ l$ ($l = \pm 0, 1, 2, 3..$) which is delivered within a numerical implementation. This task is fraught with uncertainty not least because phase is undefined where spectral amplitudes are zero [see e.g., *Jin and Eisner*, 1984]. Since the seismograms $P_{mn}(\omega)$ have been normalized to minimum phase, their phase possesses zero trend; that is, it is periodic in frequency and constant across the Nyquist frequency. As a consequence, phase does not vary significantly and is easily unwrapped. Moreover, since $P_{mn}(\omega)$ represents a minimum-phase time series, property 2 in section 2 requires that both of $S_m(\omega)$, $G_n(\omega)$ correspond to minimum-phase functions.

[24] As an alternative to the procedure outlined above, we could have chosen to deal with the power spectra of the

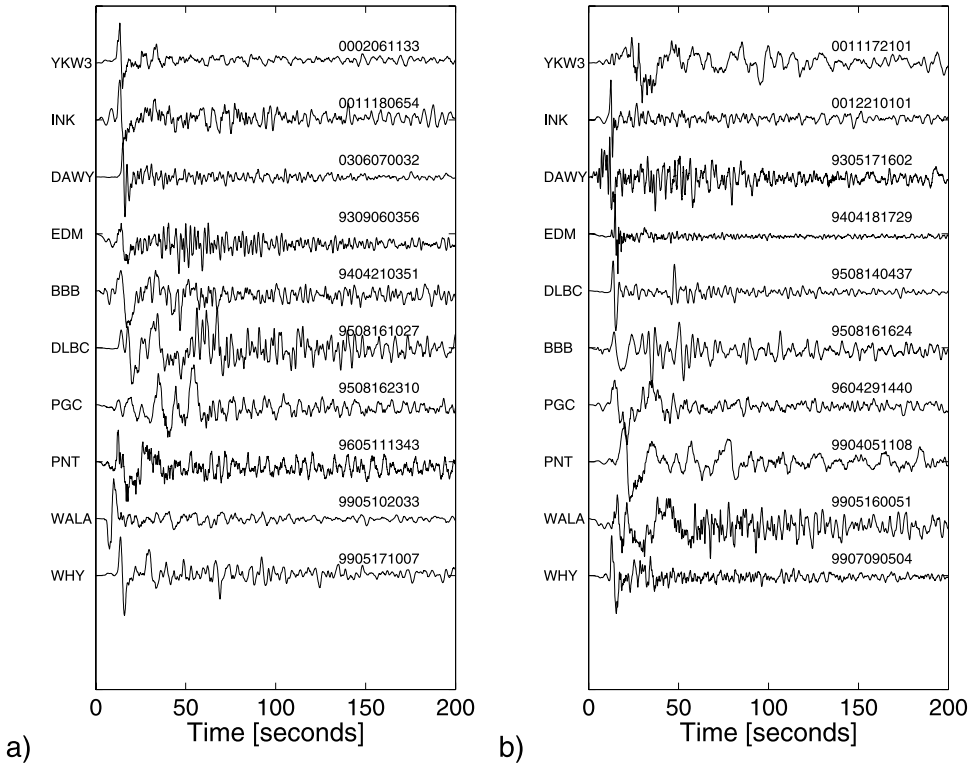

Figure 7. Papua New Guinea-western Canada seismograms. Vertical component seismograms recorded at 10 stations of the CNSN representing two suites (a) 91 *P* seismograms and (b) 85 *P* seismograms of earthquakes used in examples. Suite illustrated in Figure 7a is also used to simulate source functions for synthetic seismograms. The full complement of seismograms for both suites of events is used to demonstrate reproducibility of Green's function estimates from real data.

seismograms $P_{mn}(\omega)$*$P_{mn}(\omega)$, the sources $S_m(\omega)$*$S_m(\omega)$, and the Green's functions $G_n(\omega)$*$G_n(\omega)$, rather than the corresponding minimum phase seismograms. These spectra obey equations analogous to equations (18)–(20). Treatment of phase is rendered trivial because the phase of all quantities is identically zero, so that no unwrapping is required. The same constraint equations (21) and (23) and associated caveats apply because a delta function is at once both zero phase and minimum phase. Upon solution of the linear system, the 3-D minimum-phase, *P* component, transmission Green's function can be recovered from its spectrum using the Kolmogorov algorithm. Note that, unlike in section 4, we make no association here between the power spectrum (or in the time domain, autocorrelation) of the transmission Green's function and the corresponding reflection quantity.

[25] Our reason for preferring the minimum-phase deconvolution over that employing spectra is that augmentation of the linear system in equation (20) with additional mixed-phase components of the wave field appears to be simpler. For a given source $S_m(\omega)$, we may provide an additional two equations corresponding, e.g., to *SV* and *SH* components of the teleseismic *P* seismogram, that is,

$$\log\{S_m(\omega)\} + \log\{R_n(\omega)\} = \log\{V_{mn}(\omega)\}, \tag{25}$$

$$\log\{S_m(\omega)\} + \log\{T_n(\omega)\} = \log\{H_{mn}(\omega)\}, \tag{26}$$

respectively. The data $V_{mn}(\omega)$ and $H_{mn}(\omega)$ are defined by

$$\begin{aligned} V_{mn}(\omega) &= \mathcal{K}\{A_{mn}(\omega)S_m(\omega)\hat{w}_U^V(\omega)\} \\ &= \mathcal{K}\{\mathcal{K}\{S_m(\omega)\}\hat{w}_U^V(\omega)\} \\ &= \mathcal{K}\{S_m(\omega)\}R_n(\omega) \end{aligned} \tag{27}$$

$$\begin{aligned} H_{mn}(\omega) &= \mathcal{K}\{A_{mn}(\omega)S_m(\omega)\hat{w}_U^H(\omega)\} \\ &= \mathcal{K}\{\mathcal{K}\{S_m(\omega)\}\hat{w}_U^H(\omega)\} \\ &= \mathcal{K}\{S_m(\omega)\}T_n(\omega) \end{aligned} \tag{28}$$

where $S_m(\omega)\hat{w}_U^V(\omega)$ and $S_m(\omega)\hat{w}_U^H(\omega)$ are the raw *SV* and *SH* spectra (in this case at the *n*th receiver) and $A_{mn}(\omega)$ $S_m(\omega)\hat{w}_U^V(\omega)$ and $A_{mn}(\omega)S_m(\omega)\hat{w}_U^H(\omega)$ are the corresponding seismograms with normalized source signatures (i.e., $\mathcal{K}\{S_m(\omega)\}$), per equation (12). A second transformation to minimum phase is applied to normalize the mixed-phase impulse responses $\hat{w}_U^V(\omega)$, $\hat{w}_U^H(\omega)$ to avoid complications in phase unwrapping as described above. The solutions $R_n(\omega)$ and $T_n(\omega)$ are thus unphysical minimum-phase time series that possess the same autocorrelations and power spectra as the corresponding *SV* and *SH* components of the Green's function. These latter components can, in turn, be retrieved through multiplication by an all-pass filter, $B_n^{-1}(\omega)$, defined, e.g., for *SV* waves and a single seismogram, as

$$B_n(\omega) = \frac{\mathcal{K}\{\mathcal{K}\{S_m(\omega)\}\hat{w}_U^V(\omega)\}}{\mathcal{K}\{S_m(\omega)\}\hat{w}_U^V(\omega)}. \tag{29}$$

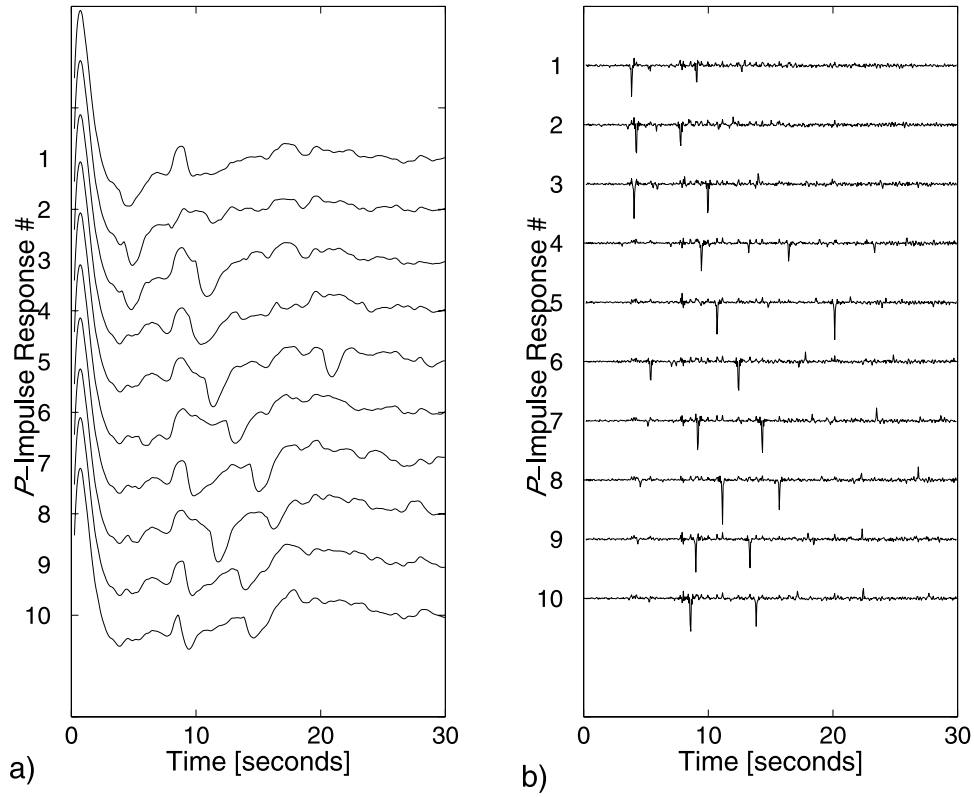

Figure 8. Synthetic multichannel deconvolution. Estimates of intramodal Green's functions derived from 100 synthetic *P* waveforms constructed from convolution of impulse responses in Figure 6 with time functions in Figure 7a and using constraints in (a) equation (21) and (b) equation (24).

The filter $B_n(\omega)$ depends only on the *P*-to-*SV* impulse response at site *n* and should thus be independent of event *m*. To mitigate the effects of noise, it is tempting to define $B_n(\omega)$ from multiple measurements *m* through a geometric average as

$$B_n(\omega) = \prod_m^M \left[\frac{\mathcal{K}\{A_{mn}(\omega) S_m(\omega) \hat{w}_U^V(\omega)\}}{A_{mn}(\omega) S_m(\omega) \hat{w}_U^V(\omega)} \right]^{\frac{1}{M}}. \quad (30)$$

$B_n(\omega)$ computed in this way is, however, mixed phase and hence we run into difficulty with phase unwrapping as described above. It is therefore simpler to form the *SV* (and *SH*) Green's function estimate through some other average, for example, the mean of the time domain waveforms constructed using the estimates of $B_n(\omega)$ acquired from each source.

6. Synthetic and Data Examples

[26] We proceed now to examine the application of multichannel source-Green's function deconvolution via minimum-phase waveform normalization through synthetic simulations and a selection of data from stations of the CNSN. In our first set of examples we prepare a synthetic data set of *P* impulse responses for 10, two-layer, 1-D, isotropic models using a reflectivity code. For each model the horizontal slowness *p* is randomly generated between 0.041 and 0.079 s km^{-1} thus representing values typical of teleseismic *P*. For simplicity we assume Poisson solids, and constant densities in the layers and underlying half-space of 2500, 2800, and 3300 kg m^{-3}, respectively. The *P* velocities and thicknesses in the first two layers are again randomly generated. The *P* velocities vary between 4.0–5.0 km s^{-1} and 5.0–6.0 km s^{-1} in the two top layers, and the *P* velocity is held fixed at 8.2 km s^{-1} in the half-space. In addition to these structural signals we insert a signal common to all of the impulse responses, that is, a constant amplitude spike at 8.0 s after the arrival of direct *P* on the vertical component on all seismograms. The final data set (Figure 6) comprises the *P* component waveforms estimated using the method of *Kennett* [1991], free-surface *P* and *S* velocities of 4.5 and 2.60 km s^{-1}, respectively, and the appropriate horizontal slownesses. Note that the direct arrival at $t = 0$ has an amplitude that is an order of magnitude larger than the later arrivals. It is omitted in Figure 6 to emphasize the scattered arrivals.

[27] Synthetic source time signatures are taken from 10 arbitrarily chosen, real seismograms recorded at 10 different Canadian National Seismograph Network stations from 10 different earthquakes in Papua New Guinea. As displayed in Figure 7a, these signatures are relatively complex and represent a range of different frequency spectra. The source signatures are then convolved with each of the 10 impulse responses to simulate a multichannel data set of 100 seismograms that are subsequently deconvolved within a system analogous to equation (20) and supplemented with constraints (21) and (23) in Figures 8a and 8b, respectively.

[28] At first glance Figures 8a and 8b look quite different, and Figure 8b appears to be a better representation of the true Green's function response as a sparse spike train. We

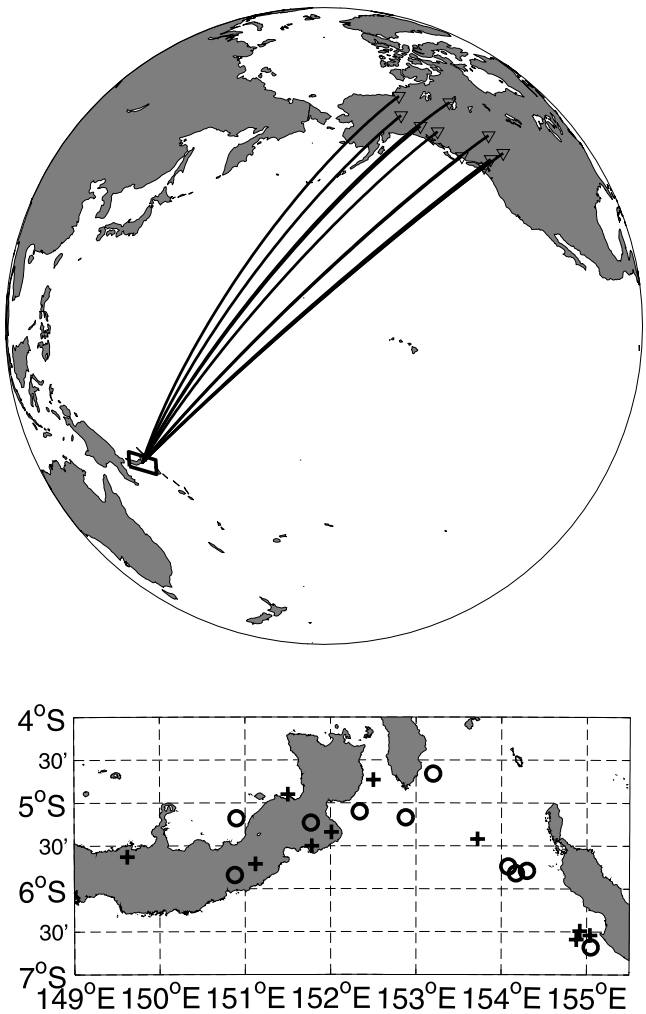

Figure 9. Locations of earthquakes and stations. (top) Location of source region and great circle trajectories from one source to each of 10 CNSN stations (inverted triangles). (bottom) Earthquake locations with two independent data sets denoted by plusses and circles.

note, however, that the positive arrival at 8.0 s is not represented in the recovery, confirming our earlier prediction that structure common to all $G_n(\omega)$ is lost using constraint (23). The Green's function response in Figure 8a is band-limited and, in particular, possesses the amplitude spectrum of the product of the individual seismogram spectra; however, it does recover the pulse at 8.0 s along with the other first-order interactions. Some residual source contamination is evident as signal with zero moveout across the section, but it is significantly smaller than the main first-order arrivals. Simple band-pass filtering of the response in Figure 8a could be applied to better balance the amplitude spectra.

[29] For observational studies, we are likely to have a less complete sampling of sources and receivers, i.e., not all receivers will record all sources. Recordings from portable field (e.g., IRIS-PASSCAL) campaigns provide a useful case in point. Limited availability and high demand for portable instrumentation generally require that such endeavors are of short duration (<1–2 years). Thus a field array is unlikely to record more than a single high-quality earthquake from any given source region on the globe. However, one or a few permanent stations with long recording histories and in close proximity to the field array should possess a considerable inventory of earthquakes representing similar source-receiver combinations (proximity of permanent station with field array is desirable to minimize directivity and other departures from the point source/convolutional model). To examine the efficacy of the multichannel deconvolution, we have employed a subset of the aforementioned data set comprising 10 events recorded by a single station (*P* impulse response 1 in Figure 6) of which one event (event 10 of Figure 7) is also recorded by the remaining nine stations. This grouping represents a total of 19 observations (versus 100 in the

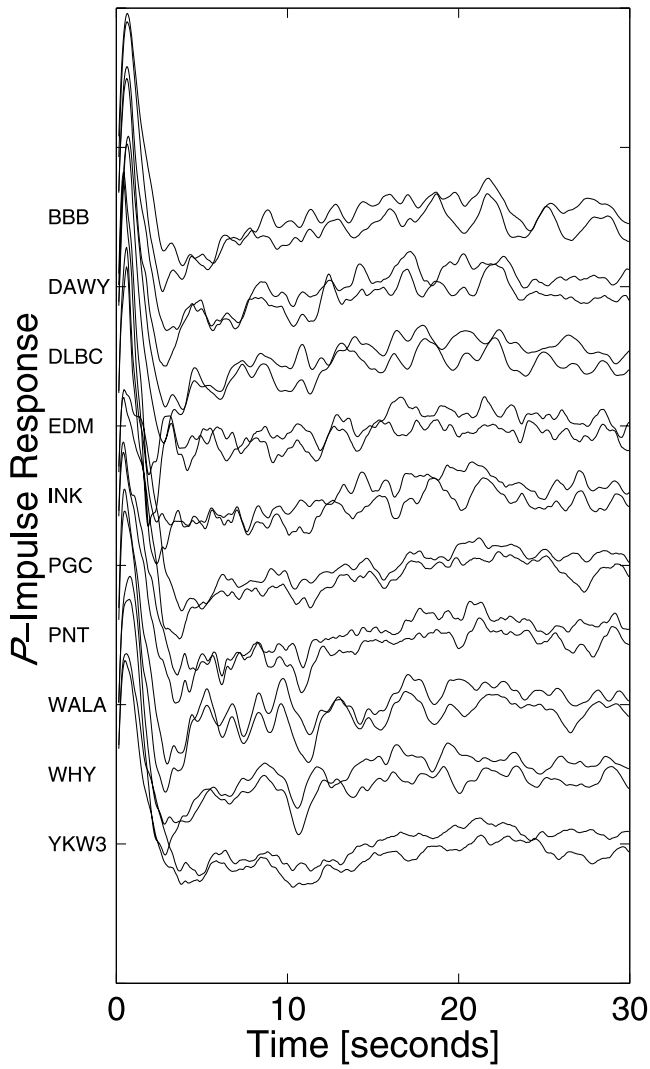

Figure 10. Multichannel deconvolution of CNSN data. Estimates of *P* component Green's functions determined using only *P* wave seismograms from two independent data sets representing Papua New Guinea earthquakes recorded at 10 CNSN stations are shown. The responses for the two data sets are slightly displaced from one another to facilitate comparison. Seismograms have been band-pass filtered between 0.1 and 8 Hz.

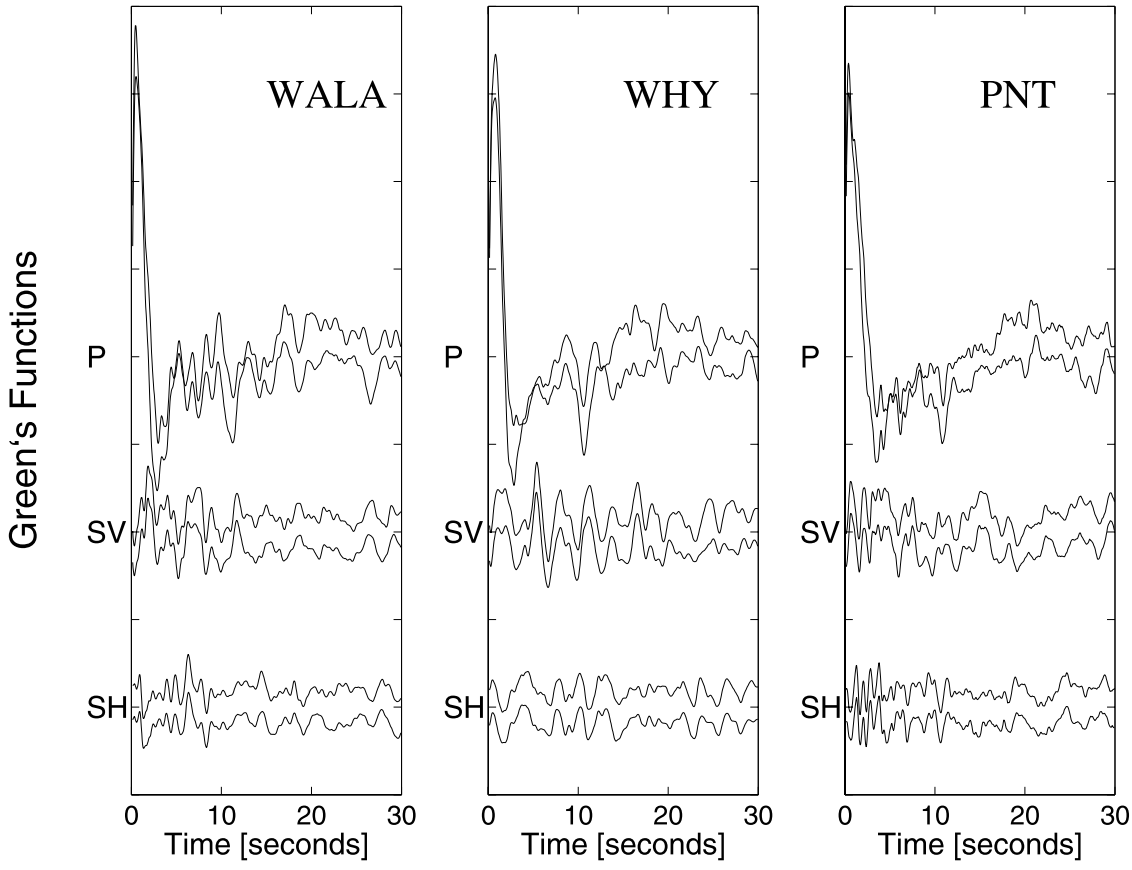

Figure 11. Multicomponent, single-station deconvolution. Estimates of *P*, *SV*, and *SH* impulse responses derived from single-station data for two suites of earthquakes in Figure 6 at stations WALA, WHY, and PNT are shown. Responses are slightly displaced from one another to facilitate comparison. Responses have been band-pass filtered between 0.1 and 8 Hz, and all show prominent negative polarity peaks near 10–11 s that are likely *P-P* reflections from the crust-mantle boundary.

original grouping) plus 1 constraint (equation (23)) to estimate 20 unknowns (10 sources and 10 impulse responses). The results of this simulation (not shown) are virtually identical to those in Figure 8a, and suggest that recordings from permanent stations are likely to provide useful calibration for portable experiments.

[30] The examples discussed to this point represent perfect data with no errors. Rather than construct synthetic noise examples that are likely to be unrepresentative of contamination present in actual data, we choose to examine the robustness of multichannel deconvolution by minimum-phase normalization through the analysis of two independent data sets representing the same set of impulse responses. These two data sets are formed from 20 earthquakes in Papua New Guinea, recorded at 10 CNSN stations (BBB, DAWY, DLBC, EDM, INK, PGC, PNT, WALA, WHY, and YKW3). The events are closely spaced relative to the propagation paths (see Figure 9) and therefore all seismograms recorded at a single station represent the same 3-D Green's function. Examples of seismograms from these 20 events are shown in Figures 7a and 7b. We divide the data set into two suites of 10 earthquakes, one comprising 91 *P* seismograms, the other 85 *P* seismograms. Figure 10 shows the *P* impulse response determined by multichannel, simultaneous deconvolution for the 10 stations using the two data sets. In general the phase match is good, although there are differences in amplitudes at some stations. Given the geographic range represented by these stations, namely, western Canada, it is possible that some inconsistency is introduced through source directivity which results in slightly different effective source signatures beneath each station.

[31] In a second example (Figure 11), we show the result of deconvolving the three components of the Green's function for stations WALA, WHY, and PNT by employing only those three-component data recorded at the respective stations within the approach embodied in equations (25)–(30). As a consequence, finite fault dimension should not have any detrimental effect on the solution. The impulse responses for all three components are very consistent between the two independent data sets and so we believe an accurate estimate of the Green's function is being recovered. Corroboration is provided through a comparison with the *SV* and *SH* receiver functions using simultaneous, frequency domain deconvolution [*Gurrola et al.*, 1995] which produces broadly similar but more variable time series (see Figure 12). In both approaches, precisely the same data sets are being used; however, the underlying philosophies are different. In receiver function analysis, the *P* and *S* component waveforms play asymmetric roles as source estimates and raw data, respectively. In contrast, all components of the wave field contribute

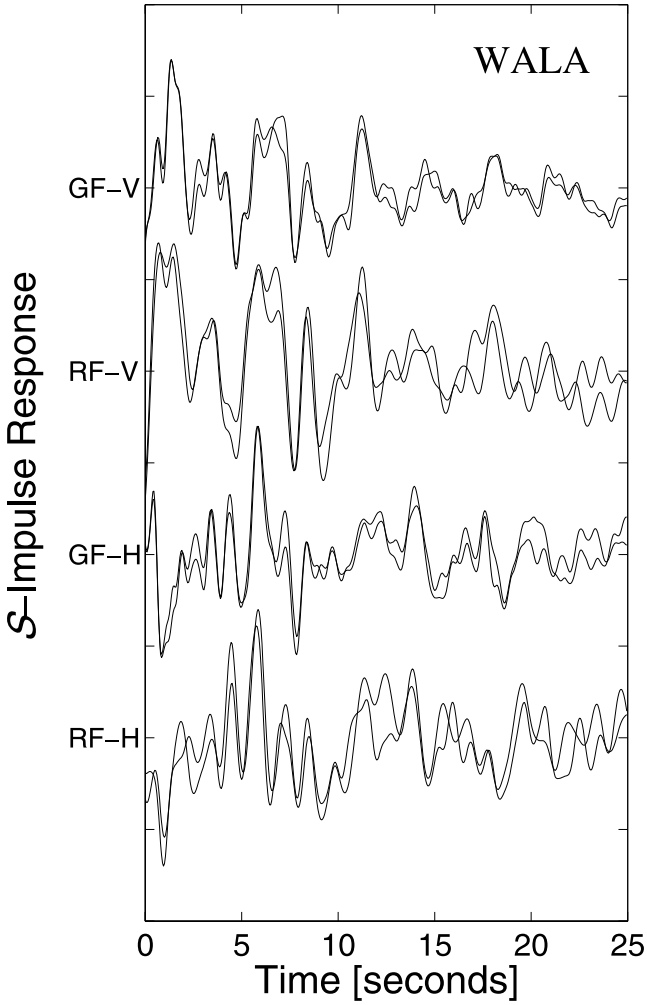

Figure 12. *SV* and *SH* components of Green's functions and receiver functions (GF and RF, respectively) at station WALA showing superposed results from the two independent Papua New Guinea data sets. Larger arrivals on both Green's functions and receiver functions correspond well, but significant differences do exist.

equally to the estimation of both Green's function and source signature in the approach described here. The consistency among all three components for the two data sets and the better accounting for source suggests that the Green's function seismograms in Figure 11 may contain meaningful information on higher- (i.e., second) order scattering (see Figure 1). In our experience to date, we see little sign of the instability that can occur, for example, in simple deconvolution via spectral division. This behavior stems from the constraint in equation (21) which, in effect, imposes a "whitening" of the source spectra akin to dampening in standard least squares deconvolution [e.g., *Oldenburg*, 1981], and from the redundancy inherent in equation (20) with multiple sources and receivers.

7. Concluding Remarks

[32] We have shown how normalization through transformation to minimum phase can be exploited to estimate the Green's function for teleseismic *P* wave fields. Our primary motivation has been the extraction of the intramodal *P*-to-*P* scattering contribution which, to our knowledge, has not hitherto been adequately characterized. We have emphasized transformation to minimum phase because it should produce accurate "transmission" Green's functions for a wide variety of laterally heterogeneous Earth models. In future work, it may prove feasible to use these Green's functions within the *Claerbout* [1968] correlation approach (or, rather, multidimensional extensions thereof, e.g., *Wapenaar et al.* [2004]) to transform transmission Green's functions into reflection impulse responses that are better suited to formal (i.e., nonlinear) inversion [e.g., *Weglein et al.*, 2003]. In the context of linearized inverse scattering the transmission response should, however, be sufficient [*Bostock et al.*, 2001]. It is encouraging to note from synthetic simulations that multichannel deconvolution based on minimum-phase normalization has potential in circumstances where many stations record few events and few stations record many events as, for example, where a permanent station is sited in close proximity to a temporary field deployment. The long history of recording at the permanent installation will afford source calibration and the generation of accurate Green's functions to be used in inversion for subarray structure and material properties.

[33] **Acknowledgments.** I am grateful to Tad Ulrych for discussion and encouragement. Reviews by Gary Pavlis, Guust Nolet, and associate editor Justin Revenaugh helped to improve presentation of the material. Figure 9 was produced using Richard Pawlowicz's M_map software. I thank the Geological Survey of Canada, Natural Resources Canada, for access to the Canadian National Seismograph Network data archive. This research was supported by NSERC research grant RGPIN 138004 and a U.B.C. Izaak Walton Killam Research Fellowship.

References

Bostock, M. G., and S. Rondenay (1999a), Migration of scattered teleseismic body waves, *Geophys. J. Int.*, *137*, 732–746.
Bostock, M. G., and S. Rondenay (1999b), Corrigendum to "Migration of scattered teleseismic body waves," *Geophys. J. Int.*, *139*, 597.
Bostock, M. G., and M. D. Sacchi (1997), Deconvolution of teleseismic recordings for mantle structure, *Geophys. J. Int.*, *129*, 143–152.
Bostock, M. G., S. Rondenay, and J. Shragge (2001), Multiparameter two-dimensional inversion of scattered teleseismic body waves: 1. Theory for oblique incidence, *J. Geophys. Res.*, *106*, 30,771–30,782.
Claerbout, J. F. (1968), Synthesis of a layered medium from its acoustic transmission response, *Geophysics*, *33*, 204–209.
Claerbout, J. F. (1976), *Fundamentals of Geophysical Data Processing*, 274 pp., McGraw-Hill, New York.
Clayton, R. W., and R. A. Wiggins (1976), Source shape estimation and deconvolution of teleseismic body waves, *Geophys. J. R. Astron. Soc.*, *47*, 151–177.
Coates, R. T., and C. H. Chapman (1990), Quasi-shear wave coupling in weakly anisotropic 3-D media, *Geophys. J. Int.*, *103*, 301–320.
Crosson, R. S., and S. R. Dewberry (1994), Receiver function estimation from short-period regional network teleseismic data using cepstral deconvolution, *Eos Trans. AGU*, *75*, 485.
Frasier, C. W. (1970), Discrete time solution of plane *P-SV* waves in a plane layered medium, *Geophysics*, *35*, 197–219.
Gurrola, H., G. E. Baker, and J. B. Minster (1995), Simultaneous time domain deconvolution with application to the computation of receiver functions, *Geophys. J. Int.*, *120*, 537–543.
Jin, D. J., and E. Eisner (1984), A review of homomorphic deconvolution, *Rev. Geophys.*, *22*, 255–263.
Kennett, B. L. N. (1983), *Seismic Wave Propagation in Stratified Media*, 342 pp., Cambridge Univ. Press, New York.
Kennett, B. L. N. (1991), The removal of free surface interactions from three-component seismograms, *Geophys. J. Int.*, *104*, 153–163.
Kolmogorov, A. (1939), Sur l'interpolation et l'extrapolation des suites stationnaires, *C. R. Acad. Sci.*, *208*, 2043–2045.

Langston, C. A. (1979), Structure under Mount Rainier, Washington, inferred from teleseismic body waves, *J. Geophys. Res.*, *84*, 4749–4762.

Oldenburg, D. W. (1981), A comprehensive solution to the linear deconvolution problem, *Geophys. J. R. Astron. Soc.*, *65*, 331–357.

Pavlis, G. (2003), Imaging the Earth with passive seismic arrays, *Leading Edge*, *22*, 224–231.

Revenaugh, J. (1995), A scattered-wave image of subduction beneath the Transverse Ranges, *Science*, *268*, 1888–1892.

Robinson, E. A., and S. Treitel (1980), *Geophysical Signal Analysis*, 466 pp., Prentice-Hall, Englewood Cliffs, N. J.

Shearer, P. M. (1991), Constraints on upper mantle discontinuities from observations of long-period reflected and converted phases, *J. Geophys. Res.*, *96*, 18,147–18,182.

Sherwood, J. W. C., and A. W. Trorey (1965), Minimum-phase and related properties of a horizontally stratified absorptive Earth to plane acoustic waves, *Geophysics*, *30*, 191–197.

Ulrych, T. J. (1971), Application of homomorphic deconvolution to seismology, *Geophysics*, *36*, 650–660.

Vinnik, L. P. (1977), Detection of waves converted from *P* to *SV* in the mantle, *Phys. Earth Planet. Inter.*, *15*, 39–45.

Wapenaar, K., J. Thorbecke, and D. Draganov (2004), Relations between reflection and transmission responses of 3-D inhomogeneous media, *Geophys. J. Int.*, *56*, 179–194.

Weglein, A. B., F. V. Araújo, P. M. Carvalho, R. H. Stolt, K. H. Matson, R. T. Coates, D. Corrigan, D. J. Foster, S. A. Shaw, and H. Zhang (2003), Inverse-scattering series and seismic exploration, *Inverse Prob.*, *19*, R27–R83.

M. G. Bostock, Department of Earth and Ocean Sciences, University of British Columbia, 2219 Main Mall,Vancouver, B. C., Canada V6T 1Z4. (bostock@geop.ubc.ca)